Hindawi
Advances in Civil Engineering
Volume 2021, Article ID 9953554, 18 pages
https://doi.org/10.1155/2021/9953554

Research Article

Investigation on the Deformation Law of Inner Waste Dump Slope in an Open-Pit Coal Mine: A Case Study in Southeast Inner Mongolia of China

Bo Cao,[1] **Shuai Wang**,[1] **Danqing Song**,[2] **Han Du**,[2] **and Weiqiang Guo**[1]

[1]*College of Mining Engineering, Liaoning Technical University, Fuxin 123000, China*
[2]*Department of Hydraulic Engineering, State Key Laboratory of Hydroscience and Engineering, Tsinghua University, Beijing 100084, China*

Correspondence should be addressed to Danqing Song; songdq2019@mail.tsinghua.edu.cn

Received 14 March 2021; Accepted 8 July 2021; Published 4 August 2021

Academic Editor: Castorina S. Vieira

The settlement and deformation of an open-pit mine waste dump were investigated by using field monitoring and numerical methods. The creep parameters of fine soil sand in the dump fill were inverted using the steady Burgers creep model, and FLAC3D software was used to simulate the dumping soil construction and development program. The results show that the settlement displacement of the dump increases with the time of dumping soil and tends to be stable after 4 years. In the creep attenuation stage of the creep process, there is a big difference between the numerical calculation and the field monitoring results in the inversion process of fine-grained soil sand parameters. In the steady-state creep stage, the numerical calculation is consistent with the field monitoring value. The height of the fill has an influence on the settlement of the fill body of the dump and the time to reach the stability. The higher the filling height is, the greater the postconstruction settlement will be, and the longer it will take to reach stability. The pushing position of the fill body has a great influence on the settlement displacement of the dump. The time and efficiency of soil discharge can be shortened by optimizing the safe distance between the filling body and the river. Based on the numerical calculation results and the empirical settlement function, an analytical method for river channel location selection of internal dump is proposed.

1. Introduction

The waste dump site is an artificial accumulation body of loose waste rock after open-pit mining [1, 2]. Open-pit mine dump can be divided into internal waste dump and external waste dump [3]. However, no matter in or out of the dump, accidents such as landslides and mud-rock flows that lead to human injury and property loss occur from time to time [4]. For example, from 1990 to 2000, under the influence of rainfall, landslides totaling about $1.54 \times 107\ m^3$ occurred in the southern and western dumps of Yongping Copper Mine in Jiangxi province, China (Figure 1(a)) [5]. In 2002, a total amount of debris flow of $3.8 \times 107\ m^3$ occurred in Nanfen Iron mine, China, under the influence of rainfall (Figure 1(b)), which caused great damage to the mine and surrounding environment [6]. Therefore, as the acceptance site for the loose body of waste rock and soil is removed from open-pit mines, the slope stability of the dump has been widely studied for a long time as a technical topic of safe production in open-pit mines [7–11].

The slope stability of open-pit mine has extremely important influence on mining and surrounding environment [12–18]. The study on slope stability of open-pit mine mainly includes the stability of working side slope and dump slope [19, 20]. At present, many research studies have been carried out on slope stability of open-pit mine [21–23]. For example, Dick et al. [24] presented a newly proposed early warning time-of-failure analysis procedure for use in real-time with ground-based radar measurements designed to be integrated in an open-pit mine's

trigger action response plan. Zhang et al. [25] investigated the shape and formation of the west boundary of the potential sliding block in an open-pit mine using the microseismic technology, DInSAR technique, and the numerical method. Liu et al. [26] investigated the dynamic stability of a mining slope in an open-pit coal mine under blasting load using numerical method and field monitoring method. Therefore, numerical calculation and field monitoring methods have become the common methods for the study of slope stability; especially the combination of the two can make the research results more reliable [27–29]. However, there are few systematic studies on the settlement and deformation of the waste dump, especially on the postconstruction settlement and deformation of the fill bulk, and the corresponding calculation methods are not mature. Generally, after the completion of the inner dump, the site may be reutilized, and some buildings are built on the upper part of the dump, so there are strict requirements on the settlement deformation of the dump. For the inner dump, the stope is close to the working area, and the filling height is generally flush with the original landform. It is very possible to place some engineering construction on the inner dump. In addition, for open-pit mines with rivers flowing through them, the need for mining will have a great impact on the river course. Therefore, it is necessary to divert the river according to the actual situation to ensure the normal exploitation of open-pit mine. However, there are few reports on the construction of river course on the inner dump. It is one of the key technologies to realize the river change project in this mine, especially to study the settlement deformation law of the bulk particles in the dump. The control and calculation requirements of soil settlement are extremely strict in the river dumping yard conversion project. Therefore, it is of great practical significance to study the settlement and deformation of the dump and master the settlement law of the bulk material and the safety and stability of the slope for the construction of the river course in the dump.

In this work, in view of the river modification project in Yuanbaoshan open-pit coal mine, the settlement and deformation regularity of the filling body of the internal dump were studied by using field monitoring and numerical methods. In the inversion of fine sand parameters, based on the classic Burgers creep model, a creep model was established for the soil filling process of the dump and the soil settlement after completion. The creep parameters of fine sand were calculated by using steady Burgers creep model, and the reliability of the inversion parameters was verified with field monitoring data. The finite-difference software FLAC3D was used to conduct numerical analysis on the filling process of fine-grained soil sand and sand gravel soil of the dump fill body, and to explore the settlement and deformation law of the dump body under the conditions of different filling body propulsion positions, thus providing a reliable basis for the deformation study of the dump body in the open-pit mine. In addition, this work innovatively constructs the river course in the inner dump and proposes an analytical method for the location selection of the river course in the inner dump.

2. Regional Overview

Yuanbaoshan open-pit coal mine is located in Chifeng City, Inner Mongolia, with an average strike length of 4.68 km and an average trend width of 2.6 km (Figure 2). The terrain of the mining area is tertiary basalt platform, the elevation range is 650–700 m, and the surface elevation range is 470–490 m.

The surface water system has the Yingjin river, which originates from Guangtou Mountain of Qilaotu Mountain in Pingquan County, Hebei Province, with a total length of 421.8 km and a basin area of 33,067 km^2. The maximum peak flow in the past years is 9840 m^3/s, and the minimum flow is 0 m^3/s. The average annual runoff is $4.297 \times 108\ m^3$, the average annual runoff is 13.6 m^3/s, and the average annual sand content is 47.5 kg/m^3. Laoha River winds through the east of the mine, with the nearest distance of 9 km to the east of the open-pit mine, which is the groundwater discharge area of the mine. The landform of the mining area is hilly, and the terrain is the highest in the basalt ridge in the northwest of the mining area, and the ridge runs northeast to southwest, as shown in Figure 3. The landform of Yuanbaoshan open-pit mine is shown in Figure 4. The slope rock mass of open-pit mine is mainly composed of tertiary, Jurassic, and quaternary strata. Lithology is mainly mudstone, sandstone, coal, carbonaceous mudstone, glutenite, etc. Through detailed investigation, it can be seen that the south side of the open-pit mine has developed a large number of joints and a number of soft intercalations of mudstone, among which the soft intercalations mainly include carbonaceous mudstone.

With the advance of the open stope, the working boundary is gradually approaching Yingjin River. By the end of 2011, the closest distance between the surface boundary of the working wall and the southern boundary of Yingjin River is less than 50 m, which is less than the safe distance stipulated in the design code, and the safety of stope is threatened. Hence, it is necessary to divert the river. The width of the riverbed and embankment is about 270 m (Figure 5). In order to reduce land acquisition and cost, part of the river is arranged on the internal dump, but the scope of the dump occupied by the river is difficult to determine. The key problem of this work is how to determine the construction scope of waste dump space occupied by river course under the premise of river course safety.

3. Deformation Analysis of the West Dump Using the Field Monitoring Method

To solve the adverse impact of Yingjinhe river on the future mining process of coal mine, the mine is faced with the problem of river course rerouting. Considering a variety of factors comprehensively, the landfill body within the dump site is selected as the river course rerouting scheme. However, the dump site will be faced with such engineering problems as settlement deformation and river course occupation after completion. For this reason, the dump west of Yuanbaoshan open-pit coal Mine was used as the test site, and a monitoring point was installed on the top of the dump using a total station as a monitoring means to analyze the

(a) (b)

Figure 1: Landslide and debris flow hazard in the open-pit mine dump: (a) landslide; (b) debris flow.

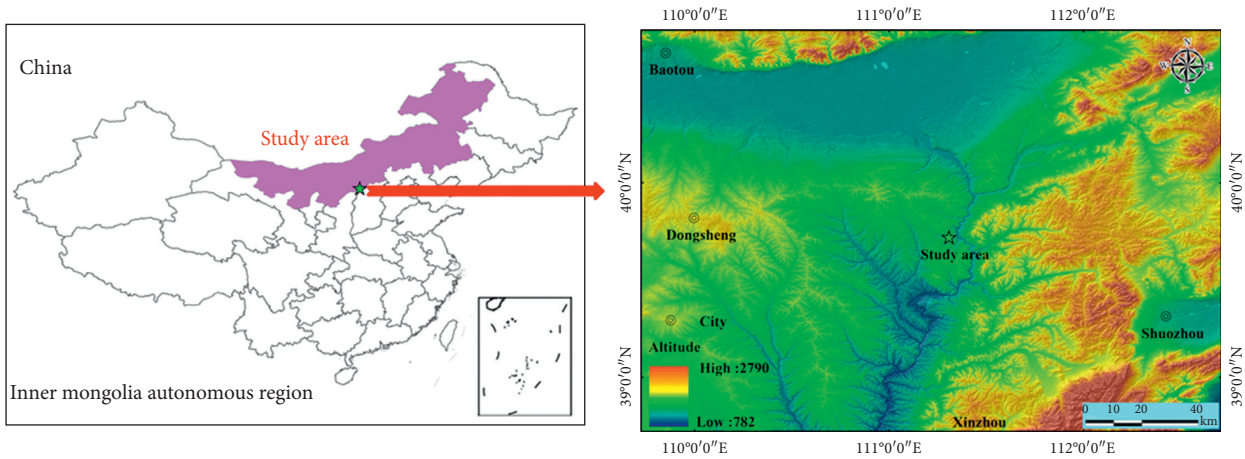

Figure 2: Location of the open-pit mine.

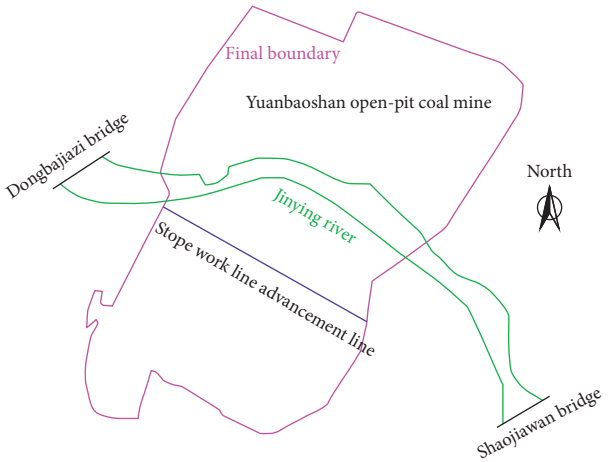

Figure 3: The Yinjin river and the open-pit mining plan.

changing law of the settlement amount of the dump fill with elevation and time (Figure 6). The settlement monitoring of the west dump and the full consideration of the filling area just completed by the dump can effectively reflect the settlement amount of the actual dumping field after completion. The west dump and the inner dump are in the same geographical location, and the soil monitoring environment of the two sites is similar.

Take the No. 1 measuring point (6-1 and 8-1) of the 6# and 8# monitoring network as an example (Figure 7), the monitoring period is from February 29, 2008, to January 27, 2015, and the settlement displacement variation of the measured point is shown in Figure 8. Figure 8 shows that the cumulative settlement displacements at the measuring points 6-1 and 8-1 were 242.0 cm and 374.0 cm, respectively, and the dumping height was 85.5 m and 132.4 m, respectively. Figure 8 shows that the settlement displacement rate of the measuring point increases rapidly in 0–1.6 years after soil discharge, decreases to a certain extent in 1.6–3.7 years, and basically tends to be stable after 4 years. In other words, the settlement displacement of the dump gradually increases with the increase of application, but its increase rate gradually decreases until it tends to be stable. In the whole soil discharge cycle (3.5 years), the average pile speed of west dump is about 50 m/a. After the completion of the dumping, the bottom of the dumping soil in the early stage gradually tends to be stable, and the upper part of the fill soil in the dump shows obvious creep settlement deformation, and the settlement displacement after completion mainly concentrates in this area. After the layered treatment of the fill body, the settlement deformation of the dump mainly occurs in the middle and upper part; that is, the layered position of the dump is closely related to the postconstruction settlement

(a) (b)

Figure 4: Schematic diagram of soil filling of the inner dump.

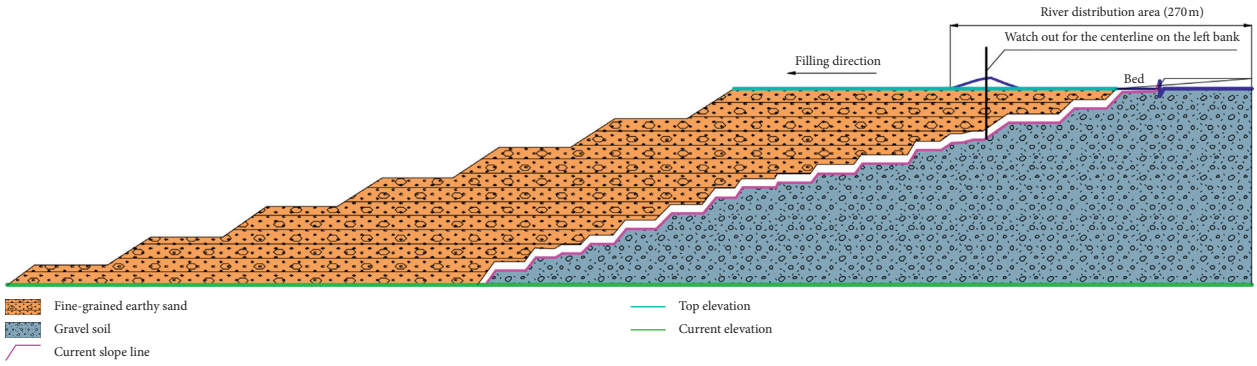

Figure 5: Schematic diagram of river layout of inner dump.

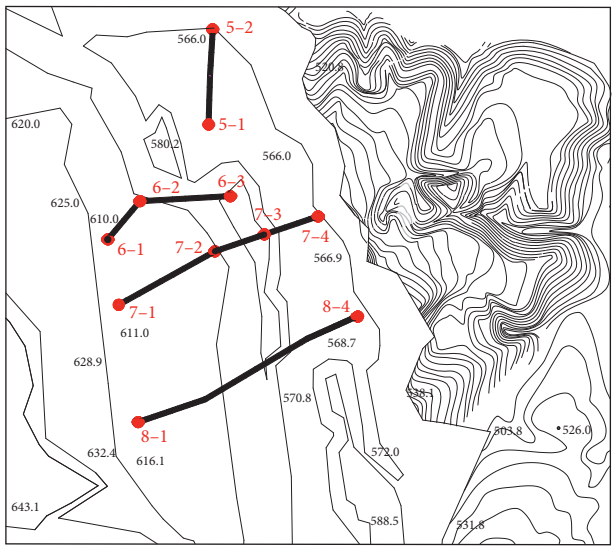

Figure 6: Distribution of subsidence monitoring sites in west dump.

[25]. However, in the process of soil discharge, due to the influence of the discharge material on the upper layer load, the soil layer in each row gradually shows creep settlement. With the increase of construction time, the settlement amount after construction decreases, and the time required for the dump to stabilize is shorter. It can be seen that the time or speed of soil discharge is directly related to the settlement after work. Since it is difficult to effectively protect the measuring points during the earth dumping construction, this monitoring work only predicts the settlement based on the dumping speed and time during the earth dumping construction, without considering the settlement during the earth dumping construction, and the impact on the river after the completion of the earth dumping should be fully considered. Hence, the following is a further prediction analysis of the settlement law of the dump.

4. Creep Characteristics Analysis of the Inner Dump

4.1. Settlement Creep Model after Construction of the Dump Fill Body. The settlement of the dump was studied using Burgers creep model. Assuming that the loading stress is the weight of soil discharge in the vertical direction of the overburden, and ignoring the influence of the weight of soil filling in the i-th layer on this layer, according to the definition of the summation method of layers, the total settlement S of the waste dump is the sum of the cumulative settlement of each layer, as follows ([30–34]):

$$S = \sum_{i=1}^{n} S_i = \sum_{i=1}^{n} \varepsilon_i H_i, \tag{1}$$

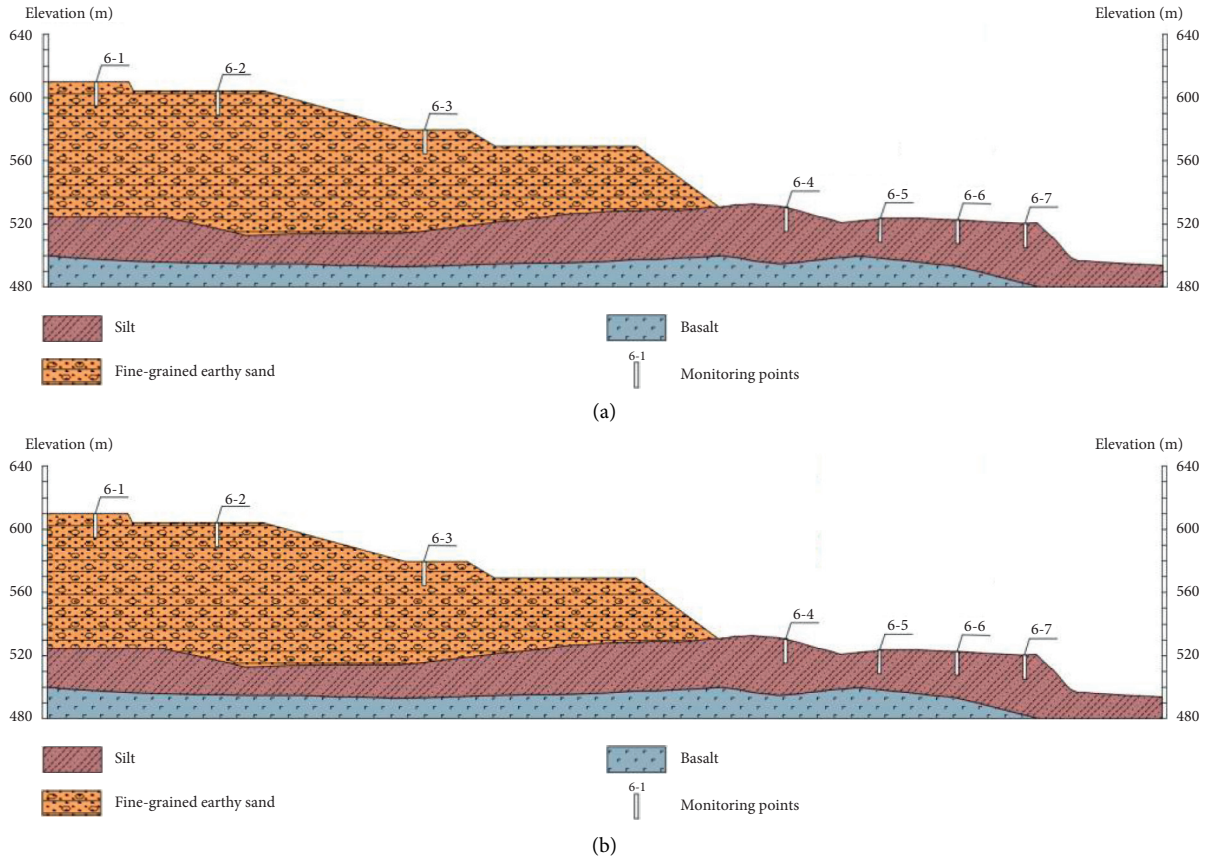

Figure 7: Section of monitoring network of west dump: (a) 6#; (b) 8#.

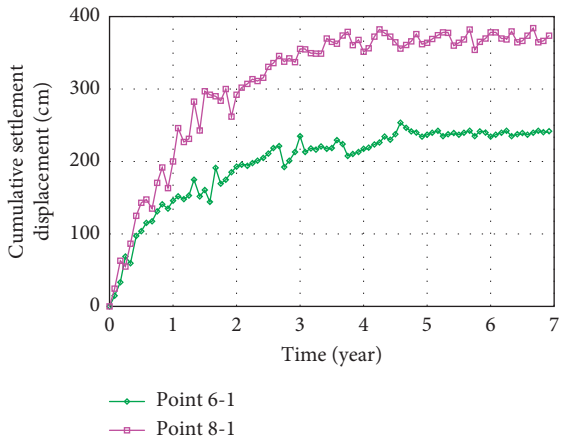

Figure 8: Settlement displacement of measuring point of measuring points 6-1 and 8-1.

where n is the number of layers of the dump. Hi is the height of the each layer. ε_i is the strain of the each layer. S is the total settlement displacement.

Assuming that the growth rate is uniform, and the fill height increases in proportion with time (Figure 9(a)), the increase rate of the fill is K_0. When the height and time are H_0 and t_0 respectively, the soil is stopped from being discharged, and the changing relation of filling height is shown in equation (2). The bulk density of the discharge material is γ, and the overburden of each layer of the fill body satisfies equation (3) [35].

$$H(t) = \begin{cases} K_0 t, & 0 \le t < t_0, \\ H_0, & t \ge t_0, \end{cases} \tag{2}$$

$$\sigma_i(t) = \begin{cases} 0, & \left(t \le \dfrac{iH_0}{nK_0}\right), \\ K_0\gamma t - \dfrac{i\gamma H_0}{n}, & \left(\dfrac{iH_0}{nK_0} < t \le t_0\right), \\ H_0\gamma - \dfrac{i\gamma H_0}{n}, & (t > t_0), \end{cases} \tag{3}$$

where $\sigma_i(t)$ is the function of the overburden increasing with time in the first layer.

The creep curve under constant stress can be divided into three stages: slow creep, constant creep, and accelerated creep. Accelerated creep is the process of rapid rock destruction. For the dispersion in a dump, the accelerated creep stage is to describe the instability process of the dump. Based on the assumption that the dump is in a stable state, and the final settlement is a constant value, the first two stages of Burgers creep are analyzed with emphasis. The creep model of Burgers is shown in Figure 9(b). The creep equation of Kelvin body and Maxwell body is as follows [35]:

$$\varepsilon_{ki} = \begin{cases} 0, & \left(t \le \dfrac{iH_0}{nK_0}\right), \\ \dfrac{1}{E_k^2}\left(\dfrac{i\gamma H_0}{n} e^{E_k/\eta_k\left((iH_0/nK_0)-t\right)} - K_0\gamma t\right) + \dfrac{1}{E_k}\left(K_0\gamma t - \dfrac{i\gamma H_0}{n}\right), & \left(\dfrac{iH_0}{nK_0} < t \le t_0\right), \\ \dfrac{1}{E_k}\left(H_0\gamma - c_k e^{-\left(E_k/\eta_k\right)t} - \dfrac{i\gamma H_0}{n}\right), & (t > t_0), \end{cases}$$

$$\varepsilon_{mi} = \begin{cases} 0, & \left(t \le \dfrac{iH_0}{nK_0}\right), \\ \dfrac{K_0\gamma t^2}{2\eta_m} + \left(\dfrac{K_0\gamma}{E_m} - \dfrac{i\gamma H_0}{n\eta_m}\right)t - \dfrac{i\gamma H_0}{nE_m} + \dfrac{i^2 H_0^2\gamma}{2n^2\eta_m K_0}, & \left(\dfrac{iH_0}{nK_0} < t \le t_0\right), \\ \dfrac{n\gamma H_0 - i\gamma H_0}{n\eta_m}t + c_m, & (t > t_0), \end{cases} \tag{4}$$

where ε_{ki} and ε_{mi} are the i-layer strain of the displacement of the Kelvin and Maxwell in Burgers model. The creep equation of steady Burgers model is as follows:

$$\varepsilon_{mi} = \begin{cases} 0, & \left(t \le \dfrac{iH_0}{nK_0}\right), \\ \dfrac{K_0\gamma t^2}{2\eta_m} + \left(\dfrac{K_0\gamma}{E_m} - \dfrac{i\gamma H_0}{n\eta_m}\right)t - \dfrac{i\gamma H_0}{nE_m} + \dfrac{1}{E_k^2}\left(\dfrac{i\gamma H_0}{n} e^{E_k/\eta_k\left((iH_0/nk_0)-t\right)} - K_0\gamma t\right) & \\ + \dfrac{1}{E_k}\left(K_0\gamma t - \dfrac{i\gamma H_0}{n}\right) + \dfrac{i^2 H_0^2\gamma}{2n^2\eta_m K_0}, \left(\dfrac{iH_0}{nK_0} < t \le T_0\right), & \\ \dfrac{1}{E_k}\left(H_0\gamma - c_k e^{-\left(E_k/\eta_k\right)t} - \dfrac{i\gamma H_0}{n}\right) + \dfrac{n\gamma H_0 - i\gamma H_0}{n\eta_m}t + c_m, & (t > T_0). \end{cases} \tag{5}$$

As the settlement of the dispersion in a dump is a gradual process with a decreasing settlement rate, the settlement displacement is approaching a certain value, and the settlement rate of steady Burgers creep model remains unchanged in the constant creep stage; hence, it is necessary to modify the linear component of steady Burgers and introduce a time-varying nonlinear component, namely, the unsteady Burgers creep model. Given that the settlement of the above dump finally converges to a constant, the viscosity coefficients in the nonlinear Kelvin model and the nonlinear Maxwell model are assumed as follows [36–45]:

$$\begin{aligned} \eta(t)_k &= A\left[\left(t - \frac{iH_0}{nK_0}\right) + R\right], \\ \eta(t)_m &= B\left[\left(t - \frac{iH_0}{nK_0}\right) + R\right]^a, \quad a \ne 1, a \ne 2, \end{aligned} \tag{6}$$

where $\eta(t)_k$ and $\eta(t)_m$ are the time-varying functions of the viscosity coefficient in Kelvin body and Maxwell body, respectively. A and B are the initial viscosity coefficient. R is a time-dependent constant; a is a compendium constant.

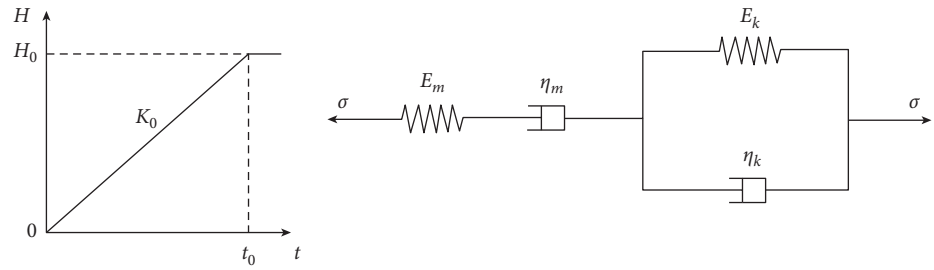

Figure 9: (a) Change of the filling height of the dump with time; (b) Burgers creep model.

The Kelvin creep equation of the ith layer of dump soil is as follows:

$$\varepsilon_{ki} = \begin{cases} 0, & \left(t \le \dfrac{iH_0}{nK_0}\right), \\ \dfrac{AK_0\gamma R^{(E_k/A)+1}}{E_k(A+E_k)}\left(t - \dfrac{iH_0}{nK_0} + R\right)^{-(E_k/A)} + \dfrac{K_0\gamma\left(t - (iH_0/nK_0) - (AR/E_k)\right)}{A+E_k}, & \left(\dfrac{iH_0}{nK_0} < t \le t_0\right), \\ \dfrac{H_0\gamma}{E_k}\left(1 - \dfrac{i}{n}\right) - \dfrac{c_k}{E_k}\left(t - \dfrac{iH_0}{nK_0} + R\right)^{-(E_k/A)}, & (t > t_0). \end{cases} \tag{7}$$

The Maxwell creep equation of the ith layer of the vertical filling dump is as follows:

$$\varepsilon_{mi} = \begin{cases} 0, & \left(t \le \dfrac{iH_0}{nK_0}\right), \\ \dfrac{K_0\gamma(2R - aR + a - 1)}{R^{a-1}B(a-1)(a-2)} - \dfrac{i\gamma H_0}{nE_m} + \dfrac{K_0\gamma}{E_m}t - & \\ \dfrac{K_0\gamma(2R - aR + a - 1)}{B(a-1)(a-2)}\left(t - \dfrac{iH_0}{nK_0} + R\right)^{1-a}, & \left(\dfrac{iH_0}{nK_0} < t \le t_0\right), \\ c_m - \dfrac{\gamma H_0}{B(a-1)}\left(1 - \dfrac{i}{n}\right)\left(t - \dfrac{iH_0}{nK_0} + R\right)^{1-a}, & (t > t_0). \end{cases} \tag{8}$$

According to equations (6) and (7), the nonlinear Burgers creep equation is as follows:

$$\varepsilon_i = \begin{cases} 0, & \left(t \le \dfrac{iH_0}{nK_0}\right), \\ \dfrac{AK_0\gamma R^{(E_k/A)+1}}{E_k(A+E_k)}\left(t-\dfrac{iH_0}{nK_0}+R\right)^{-(E_k/A)} + \dfrac{K_0\gamma\left(t-(iH_0/nK_0)-(AR/E_k)\right)}{A+E_k} - \dfrac{i\gamma H_0}{nE_m} + \dfrac{K_0\gamma}{E_m}t & \\ +\dfrac{K_0\gamma(2R-aR+a-1)}{R^{a-1}B(a-1)(a-2)} - \dfrac{K_0\gamma(2R-aR+a-1)}{B(a-1)(a-2)}\left(t-\dfrac{iH_0}{nK_0}+R\right)^{1-a}, & \left(\dfrac{iH_0}{nK_0} < t \le t_0\right), \\ \dfrac{H_0\gamma}{E_k}\left(1-\dfrac{i}{n}\right) - \dfrac{c_k}{E_k}\left(t-\dfrac{iH_0}{nK_0}+R\right)^{-(E_k/A)} - \dfrac{\gamma H_0}{B(a-1)}\left(1-\dfrac{i}{n}\right)\left(t-\dfrac{iH_0}{nK_0}+R\right)^{1-a} + c_m, & (t > t_0). \end{cases} \tag{9}$$

According to equation (1), when time tends to infinity, the total settlement amount of the dump is the cumulative sum of each layered compressed settlement, and the total settlement amount after construction is the final cumulative total settlement of the dumping soil minus the settlement amount when the dumping is completed, as follows:

$$S_\infty = \lim_{t\longrightarrow\infty}\sum_{i=1}^{n} S_{i\infty} = \lim_{t\longrightarrow\infty}\sum_{i=1}^{n}\varepsilon_i H_i = \lim_{t\longrightarrow\infty} H_i\sum_{i=1}^{n}\varepsilon_i, \tag{10}$$

where $S_{pc\infty}$, S_∞, and S_{t0} are, respectively, the total settlement after work, the final cumulative settlement of the discharged soil layer, and the settlement when the discharged soil is completed. $\varepsilon_{t_0 i}$ is the strain of the layer when the discharged soil is completed.

4.2. Deformation Parameter Regularity Law of Dump Filling. The Burgers creep model in FLAC3D was used to analyze the settlement and deformation of the fill body in the dump. Based on the monitoring data of the settlement of the dump, the creep parameters of fine-grained soil sand were obtained and used in the calculation of creep settlement of the dump. In order to verify the validity of the creep parameters, the settlement data of measuring point 6-1 was taken as the research object to obtain the creep parameters of fine soil sand. Meanwhile, the creep parameters obtained were used to further verify and analyze the creep characteristics of measuring point 8-1. The validity of creep parameters is further verified by comparing the analysis results of measuring point 8-1 with the settlement displacement monitored on-site.

To simplify the 6# monitoring network profile appropriately, the lower part of the discharged material is the original layer composed of basalt, silty soil layer, and high compactness. Only the settlement of the discharged material is considered. Rigid treatment is also applied to the original formation. The simplified section of no. 6 monitoring network is shown in Figure 10. The dumping height was divided into 10 layers on average, the dumping height at the measuring point 6-1 was 85.5 m, the dumping velocity k0 was about 50 m/a, and the bulk density of the dumping material was 16.3 kN/m^3. Based on the Burgers creep model, the lower layer of the filling body will have settlement displacement under the load of the material discharging from above, including the compression settlement (instantaneous elastic deformation and plastic deformation) of the material during the discharging process and the creep of the filling body after the discharging. The settlement deformation at the measuring point 6-1 is postwork creep. Parameter inversion was carried out using the steady Burgers model obtained in the previous study.

According to equation (8), the settlement displacement of each layer is superposition, and the settlement displacement of the measured point 6-1 (Figure 8) is analyzed by regression with the postwork settlement calculation formula ($t > T_0$). C_m and E_m can be obtained further from the settlement deformation of the dump fill ($t = T_0$), and the creep parameters of Burgers are shown in Table 1. The fitting curve of the creep model with measuring point 6-1 Burgers is shown in Figure 11. The horizontal axis and the vertical axis are, respectively, the dumping time and the settlement displacement of the measured point after completion; that is, the postconstruction settlement monitoring began in 1.71 after dumping. Figure 11 shows that the fitting curve of measuring point 6-1 in the west dump site is in good agreement with the on-site monitoring data of measuring point, and the fitting coefficient is as high as 0.982. Therefore, the creep parameters obtained by inversion can better reflect the creep process of measuring point 6-1.

In 2008, for open-pit coal mine based on the status quo of the river across the stope, and in the future in the process of mining, the river is bound to affect the direction of mining, mine will sooner or later face reelection river, and the river location choice is limited by a regional environment; consider within the earth to fill body reelection scheme, for the channel position is currently believed to be the best solution. This scheme also faces many technical problems, such as the differential settlement of the dump after construction and the range of the dump within the river occupation. Therefore, the

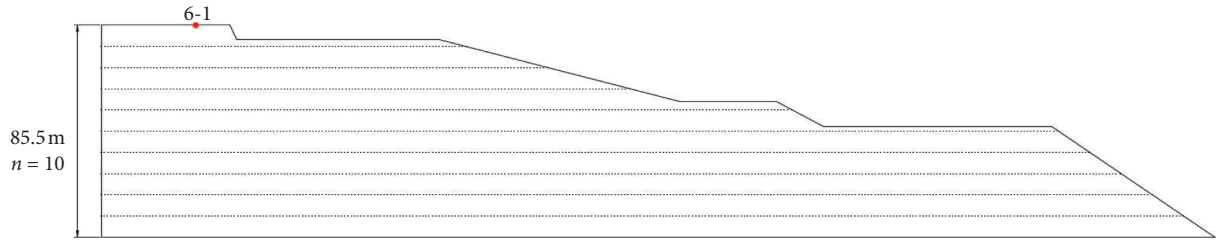

Figure 10: Simplified calculation diagram of 6# monitoring network of west dump.

Table 1: Creep parameters of fine-grained soil sand inverted from monitoring point 6-1.

E_k (GPa)	E_m (MPa)	η_k (GPa·d)	η_m (GPa· d)	c_k	c_m
1.42	13.5	505.6	492.3	2.27×10^8	−0.12

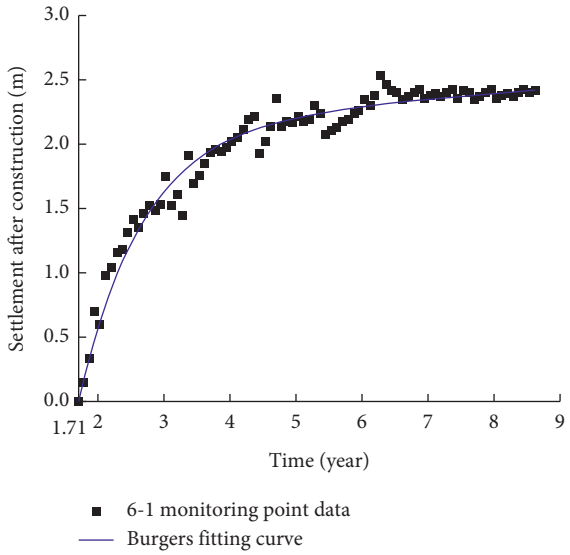

Figure 11: Fitting curve of measuring point 6-1 in west dump.

leaders of the mine decided to take the newly completed west dump as the test site and set several monitoring points at different heights and positions on the top of the dump to master the relationship between the postconstruction settlement amount of the dump fill and time and height. The monitoring of deformation and settlement can not only provide reference materials and empirical data for the design, construction, and scientific research of the filling body involved in the project of transforming the river, but also provide a practical basis for slope stability of other dump sites in the mine. Figure 3 shows the settlement monitoring points on the top part of the west dump, with a total of 11 points. In the settlement monitoring of the west dump site, the filling area just completed is considered in the layout of monitoring points, which can effectively reflect the settlement amount after the completion of the actual dump site. Because the filling body of the inner dump has not been backfilled, the settlement monitoring data of the soil of the inner dump cannot be obtained temporarily. Mine subsidence of soil changes in factors, such as rain, heavy rain, or heavy rain, within the west mine and mine, is in the same location, the monitoring of soil environment was similar, or caused by rainfall and soil consolidation settlement; on the west mine, monitoring the settlement means to reflect on the monitoring data. Therefore, taking the west dump as the test site can reflect the settlement trend of the soil in the inner dump to some extent.

Taking 8# monitoring network as the research object, the corresponding numerical calculation model was established by FLAC3D (Figure 12), and the creep parameters obtained by inversion were used for numerical calculation. The filling body of the dump was loaded in layers with Burgers creep model. The comparison of numerical calculation and field monitoring results is shown in Figure 13. Figure 13 shows that the fitting degree of numerical calculation and monitoring results is poor; especially there is a big gap between the numerical results and monitoring results in the attenuation creep stage. However, when entering the steady-state creep stage (6.25 years later), the field monitoring results and the numerical results are in good agreement, and the settlement volume gradually tends to be stable. At this time, the field monitoring value and the numerical calculation value are about 3.71 m and 3.83 m, respectively, with an error of about 0.12 m. Although there is a certain difference in the fitting degree between the numerical results and the actual monitoring results in the process of soil discharge (attenuation creep stage), when the settlement volume tends to be stable, the two results are basically the same, with an error of only 4.3%. When the river is located in the upper part of the dump, the settlement deformation caused by the dead weight of the dump is the main factor affecting the river safety. Therefore, the creep parameters obtained from the on-site monitoring data of measuring point 6-1 were used to invert and applied to the monitoring network of No. 8 to further verify the reliability of the creep parameters obtained by inversion. This parameter can describe the creep process of fine-grained soil sand.

4.3. Fill Profile and Creep Model Selection. The settlement deformation and difference settlement of the inner dump after construction cannot be ignored; especially the distance between the dump and the river is close, which requires that the settlement deformation of the fill body of the dump after completion should be controlled within a certain range. The

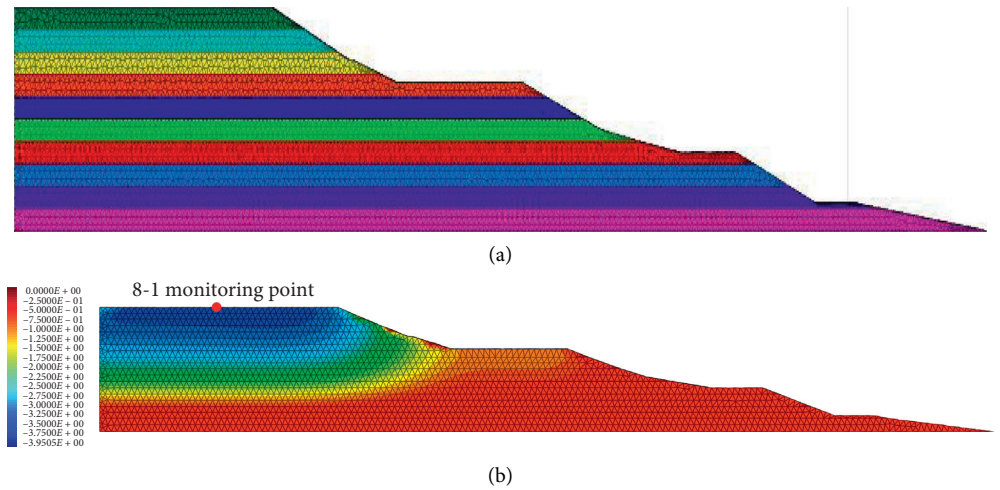

Figure 12: Calculation model and cloud map of monitoring network 8#: (a) calculation model; (b) settlement calculation cloud map.

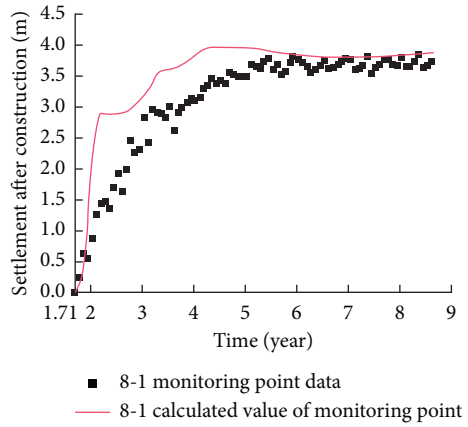

Figure 13: Comparison of observed value and numerical calculation value of monitoring point 8-1.

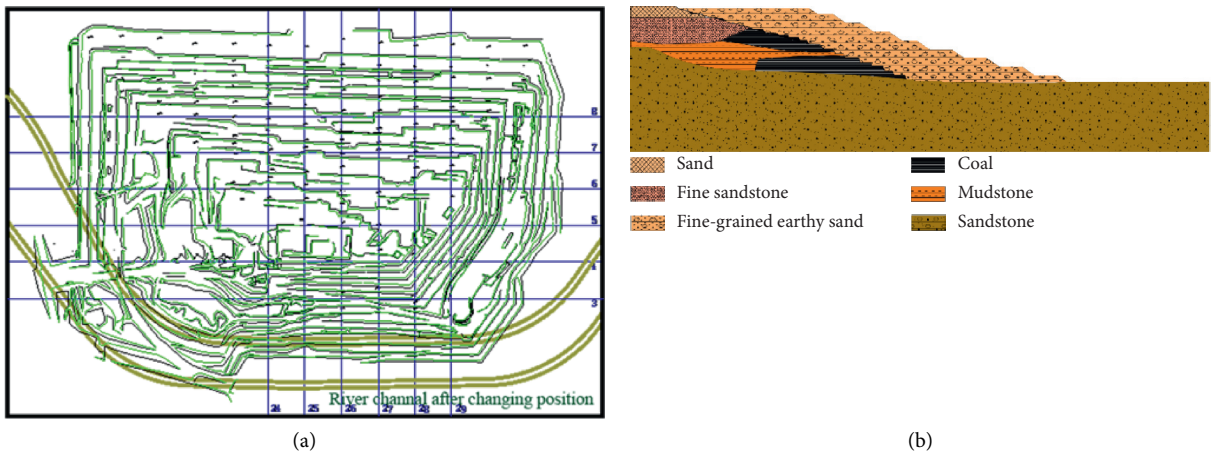

Figure 14: (a) Plan of the south side slope; (b) formation and material distribution of 26# profile.

plan of the south side of the open-pit mine is shown in Figure 14(a). Section no. 26 of the South side is taken as an example (Figure 14(b)). A numerical calculation model is established by using FLAC3D to simulate the postconstruction settlement deformation of the dump fill body. The section size of No. 26 section is 1000×400 m (length × width). The filling body was composed of fine clay sand, and numerical calculation was carried out using

Burgers creep model. The creep settlement equivalent parameters of the fill were obtained by using Burgers creep model to invert the monitoring data of the field measuring points in No. 26 section. The sand and gravel soil is the dumping cushion, and its influence on the settlement and deformation of the dump cannot be ignored. The fingers-hyperbolic mixed creep model based on the secondary development of FLAC3D is used to simulate the sand and gravel soil, and the laying thickness is 6 m.

Numerical simulation was carried out for the filling process of the dump filling body. The specific steps are as follows: (1) draw a typical section in AutoCAD, import the model into RHINOCEROS, establish a false 3d model, and divide grid nodes reasonably. (2) The above model was embedded into FLAC3D by Rhinoceros-FLAC3D. The numerical calculation model of No. 26 section in south side slope is shown in Figure 15. In order to speed up the completion of the platform at the top of the slope of the dump and reduce the settlement deformation after completion of the dump, the entire process of soil discharge is regarded as a process of uniform soil discharge. Fine soil sand units are loaded 46 times at a loading speed of 2 times, and the loading creep operation cycle is 40 days per time. The process of soil discharge is shown in Figure 16. In order to further study the creep characteristics of the displacement location of the fill body, a number of measuring points were arranged on the top of the dump, with the measuring points spaced at 20 m apart. The sloping top area was divided into area A and area B, in which area A included measuring points A1–A10. The B region includes the measuring points B1–B10. The construction period of the inner dump is about 5 years.

4.4. Analysis of Postconstruction Settlement Characteristics of the Fill. The area with the greatest distance from the river dumping volume is zone A. Hence, the settlement deformation in this area has an important influence on the settlement deformation after the river diversion. Taking five measuring points (A2, 4, 6, 8, and 10) in area A as example, the settlement and deformation rule of this area was studied. The postconstruction settlement displacement and settlement deformation cloud charts of areas A and B are shown in Figures 17 and 18. Figure 18(a) shows that the settlement displacement of the measured point of the fill body increases with the increase of the dumping time. When the dumping time reaches a certain value, there is a certain stable value in the settlement displacement area of different measuring points of the filling body. However, the settlement displacement at different measuring points takes different time to reach the stable value. In addition, Figure 17(a) also shows that when the dumping time is 600 days, the settlement displacements of the measuring points (A2, 4, 6, 8, and 10) in area A are about 104%, 82%, 67%, 61%, and 60% of the final settlement displacements, respectively. When the dumping time is 1200 days, the settlement displacements of these measuring points are about 96%, 95%, 88%, 87%, and 86% of the final settlement displacements, respectively. Meanwhile, Figure 17(a) shows that the postwork settlement

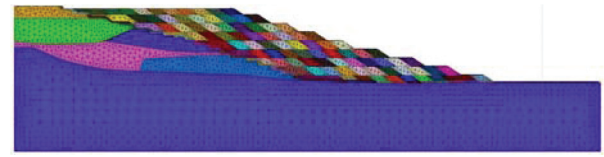

Figure 15: Numerical calculation model of 26# profile on the south side slope.

displacements of the five measuring points (A2, 4, 6, 8, and 10) in area A are different. It can be seen that the settlement rate of each measuring point decreases in the same postwork time; that is, the higher the filling height, the longer the time to reach stability, the slower the settlement, and the higher the postwork settlement.

Area B belongs to the reserved area to ensure the safety of river dumping. Take five measuring points (B2, 4, 6, 8, and 10) in area B as an example to study the settlement and deformation characteristics of this area. Figure 17(b) shows that the settlement displacements at different measuring points in area B increase with the increase of time, and when the time reaches a certain value, the settlement displacements also tend to a certain stable value. The settlement and deformation law of the filling body in areas A and B is similar. The higher the displacement height of the fill body, and the longer the data needed for the settlement displacement to reach the stable value, and the slower the settlement deformation. In addition, taking the displacement position pushed to the measuring point A6, A8, A10, B2, B4, B6, B8, and B10 as an example, the influence of the displacement position on the settlement in area A was studied. The variation characteristics of settlement displacement at the measuring point along with the advance position of dumping soil are shown in Figure 19. Figure 19 shows that the settlement displacement at each measuring point tends to be stable when the dumping time is about 10 years. Taking measuring points (A2, 4, 6, 8, and 10) in area A as an example, when the settlement displacement of each measuring point tends to be stable, the observed values of settlement displacement are 0.36, 0.68, 0.87, 0.94, 1.08, and 1.33 m, respectively. Taking 80% of the settlement displacement tending to be stable as the boundary point, the influence of different pushing positions of the filling body on the settlement deformation of the measured point of the dump was studied. When the displacement position is the measuring point in area A (A6, 8, and 10) and the measuring point in area B (B2, 4, 6, 8, and 10), the settlement displacement of the measuring point A2 in the filling body is about 0.21, 0.36, 0.37, 0.33, 0.34, 0.34, 0.34, and 0.39 m, respectively. When the displacement position is A8 and A10, the settlement displacement of A2 shows a rising trend, and its settlement displacement exceeds 80% of the total settlement displacement, which indicates that the postindustrial settlement of the measuring point A8 at the displacement position has met the settlement deformation requirements. Similarly, the postconstruction settlement of the fill body has met the settlement and deformation requirements when the dumping and pushing positions are B2, B6, B8, and B10. Therefore, reasonable optimization of

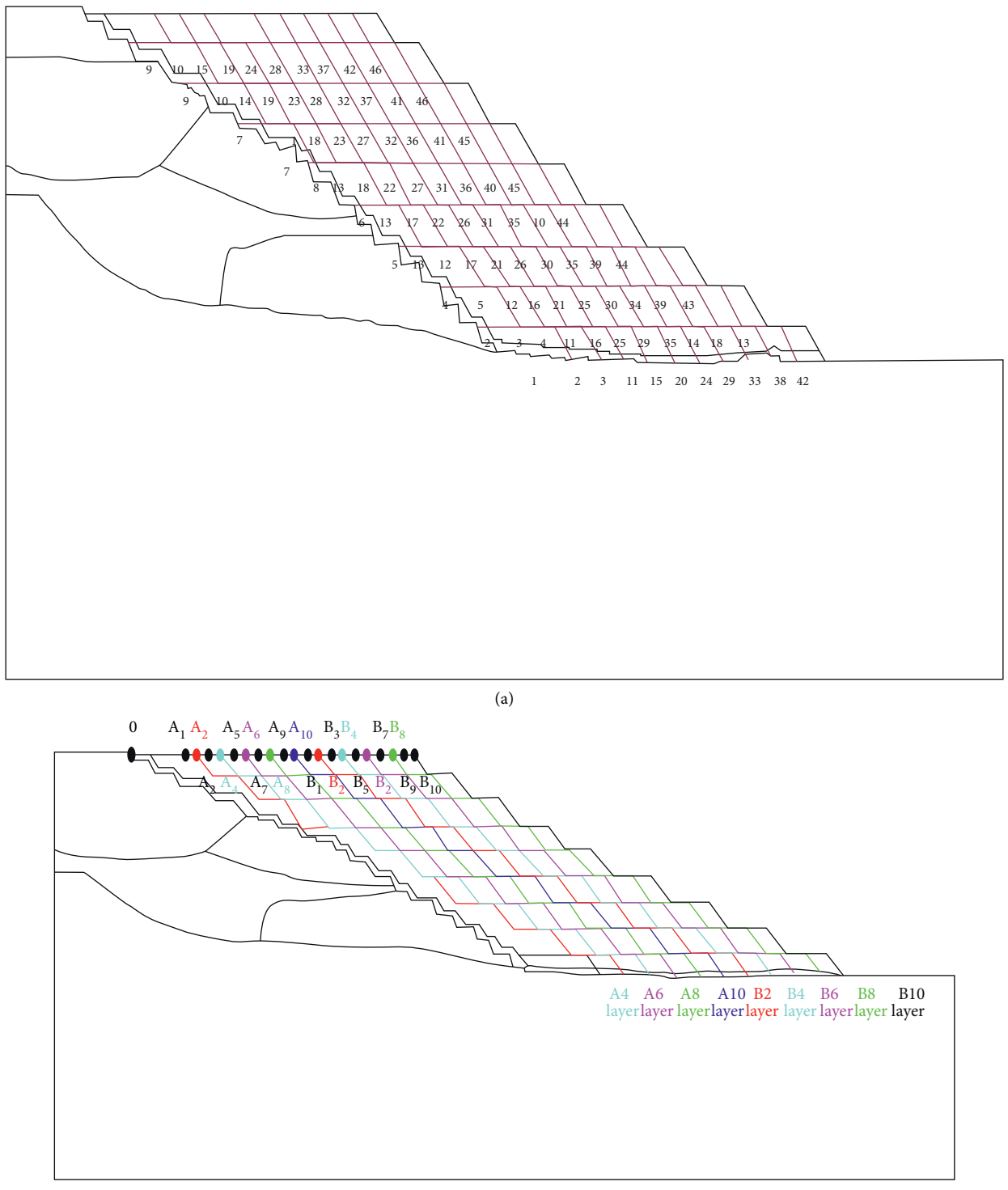

Figure 16: Backfill sequence grouping diagram of the dump: (a) the backfill sequence; (b) drainage and propulsion sequence.

the safe distance between the filling body of the internal dump and the river is an effective way to shorten the dumping time and accelerate the realization of the internal dumping. Under the condition of ensuring the stability of the filled soil slope, when the maximum locations of the waste dump occupied by the river and river embankment construction are the monitoring points A2, A4, A6, A7, A8, and A10, respectively, it is suggested that the monitoring points A8, B2, B6, B8, and B10 shall be the monitoring points for soil discharge and propulsion. The corresponding distances from O are 230, 310, 390, 430, 470, and 470 m, respectively.

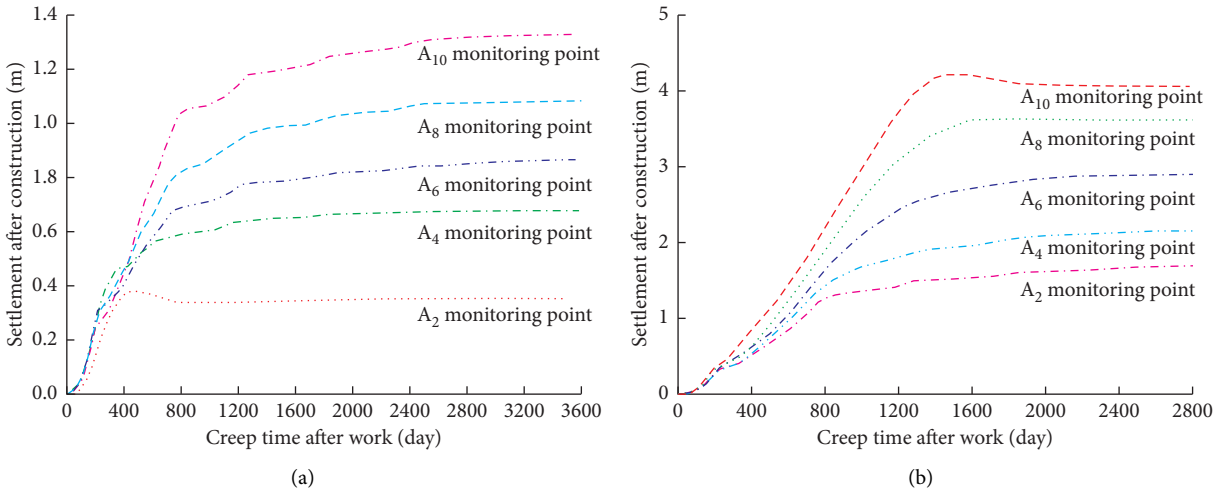

Figure 17: Postconstruction creep settlement of the monitoring point of the filling body: (a) A zone; (b) B zone.

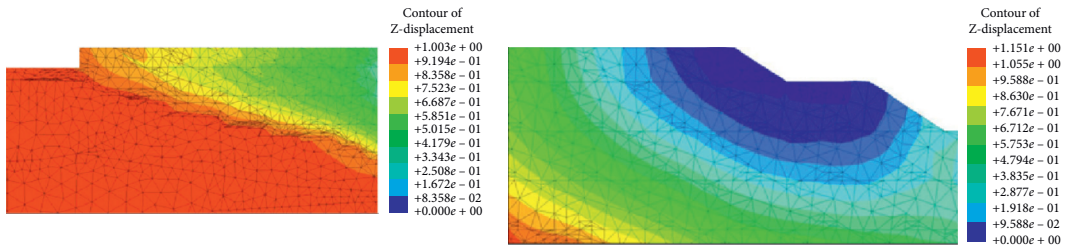

Figure 18: Postconstruction settlement cloud maps of fill body: (a) A zone; (b) B zone.

5. Selection of River Channel Reconstruction Scope above the Fill Body of the Inner Dump

The main construction task of the river reform project is to change the current river course of Yingjin River from the mining scope of Yuanbaoshan open-pit coal mine without affecting the safety of the river, so as to ensure the mining of the open-pit coal mine. Strict control of soil settlement at the bottom of the river course is the key to the river reform. However, different dumping heights will result in different settlement after construction; hence, it is particularly important to select an appropriate scope for river course construction. Based on certain assumptions, the formula of settlement amount changing with time after completion of soil filling in the dump [36] is

$$w(t) = \frac{\gamma K_0^2}{c^2 E_{ss}} e^{-(cH_0/K_0)} + \frac{\gamma K_0 H_0}{cE_{ss}} - \frac{\gamma K_0^2}{c^2 E_{ss}} - \left(\frac{\gamma K_0^2}{c^2 E_{ss}} e^{-(cH_0/K_0)} + \frac{\gamma K_0 H_0}{cE_{ss}} - \frac{\gamma K_0^2}{c^2 E_{ss}}\right) e^{-ct}. \tag{11}$$

The main parameters to be determined in the empirical function are the increase rate K_0, sink rate coefficient c, bulk density, and final compression modulus E_{ss}. The bulk density of fine-grained sand is 16.3 kN/m^3. The final compression modulus $E_{ss} = 0.035$ MPa, and the increase rate K_0 is 0.0656 m/d. The settlement velocity coefficient C corresponds to the fill height H_0, as shown in Table 2 and Figure 20.

The nonworking steps of section No. 26 are simplified (Figure 21) and regarded as the linear slope surface. Assuming that the original river geomorphology and filling boundary are changed as the origin of coordinates, any point Bi in area B (or area A) is selected, and its distance from the origin is x, then the filling height at Bi point can be represented by the distance x from the origin. The calculation

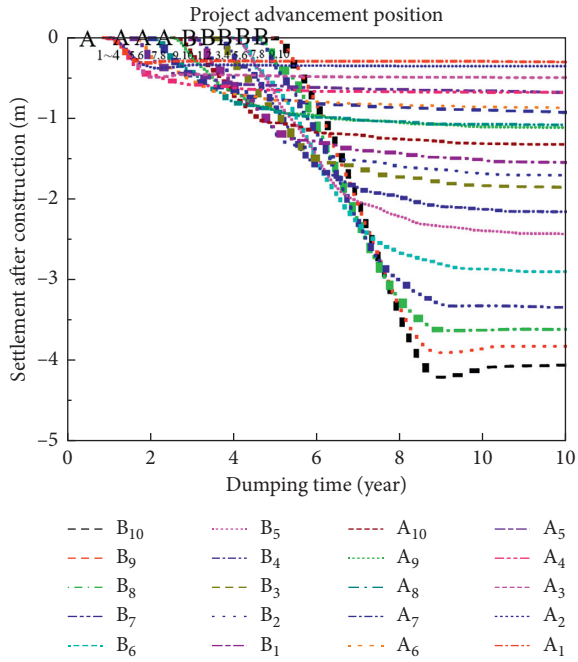

Figure 19: Postconstruction creep settlement diagram of different monitoring points.

Table 2: The maximum position of the settlement standard and the corresponding filling propulsion position.

Intersection point no.	Maximum position of standard settlement (m)	Position of fill propulsion (m)	Time
x_1	84	94	Construction period (1 year)
x_2	145.6	188	Construction period (2 year)
x_3	208.7	282	Construction period (3 year)
x_4	274	376	Construction period (4 year)
x_5	340.9	470	Construction period (5 year)
x_6	374.6	470	Intermission period (0.5 year)
x_7	407.2	470	Intermission period (1 year)
x_8	442.4	470	Intermission period (1.5 year)

formula of postconstruction settlement at any position on the top of the dump fill body is as follows:

$$w(t,x) = \left(0.516x^{0.962}e^{-0.808x^{0.519}} + 0.413x^{1.482} - 0.516x^{0.962}\right) \times \left(1 - e^{-10.51t\cdot x^{-0.481}}\right) \times 10^{-3}. \quad (12)$$

In order to compare the error of empirical function calculation value and numerical calculation value, the creep curves of empirical function calculation value and numerical calculation value of five monitoring points (A2, A6, A10, B2, and B6) are listed as shown in Figure 22. The absolute errors of their empirical function values and numerical values are 9.85%, 3.44%, 15.96%, 10.8%, and 8.18%, respectively. The creep law of each monitoring point is determined by the empirical function calculation, although there are errors in the numerical calculation to some extent, the settlement deformation of the filling body in the actual dump site is affected by many factors, and this method can be used to roughly estimate the settlement deformation of the filling body, which has certain guiding significance for the implementation of the river reform project. Moreover, Figure 23 shows that the filling period of the filling body is 5 years, and the filling location is different for different construction times. Moreover, with the advancement of different filling locations, the settlement amount after the work at the same location keeps increasing and finally converges to a certain value. From the settlement curve form during the construction period, the value of tm has a direct impact on the settlement of the overburden soil under the river and is also related to the structural safety of riverbed protection.

According to the "Design code for rolled earth-rock dam, China" (SL274-2001), the settlement of dam body and embankment foundation is required, and the construction of

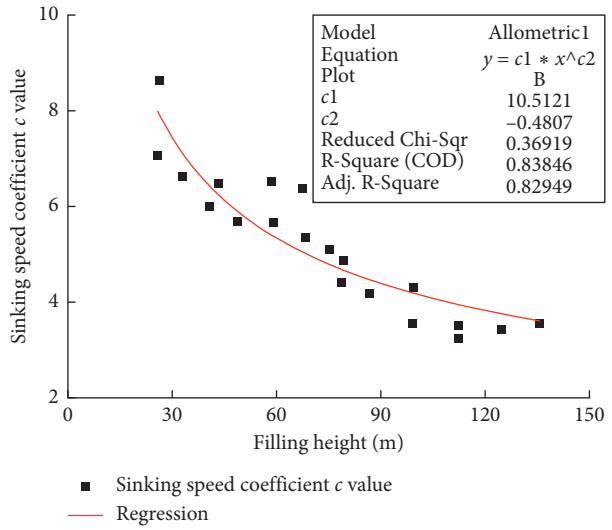

Figure 20: Relationship between subsidence velocity coefficient and fill height.

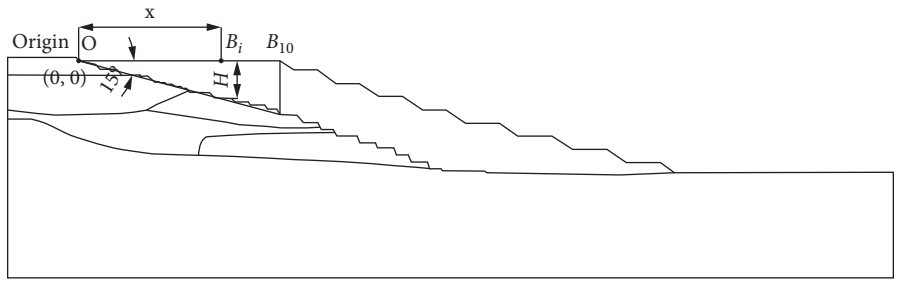

Figure 21: The geometric relationship between the fill height of section 26# and the propulsion position.

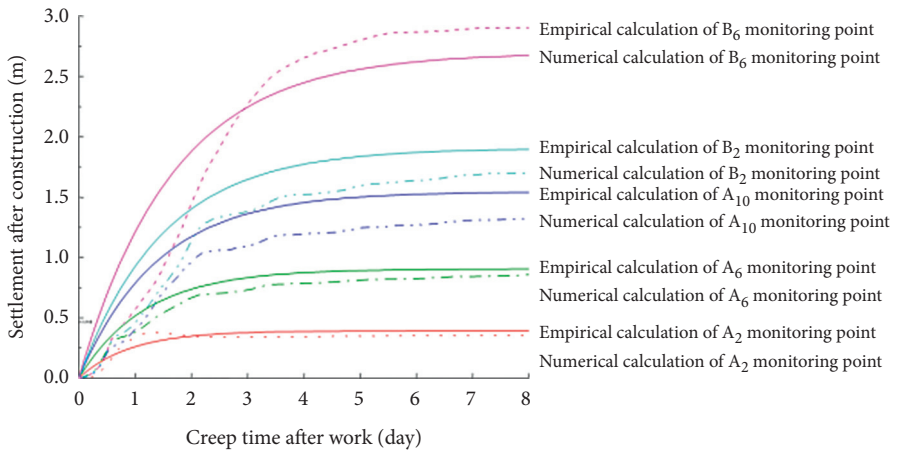

Figure 22: Comparison of numerical calculation and empirical function calculation.

river course on the inner dump is the first time at home and abroad. At present, there is no clear stipulation on the settlement standard of river course and river lift on the internal dump fill body. This work refers to the settlement standard of earth and rockfill dam, and the settlement amount after construction should not be more than 1% of the dam height. Soil discharge height $H_0 = 0.268x$, according to the requirements of the code: $M(x) \leq 0.00268x$. $M(x)$ represents the residual settlement at different positions as the filling position advances. Figure 24 shows that the curve

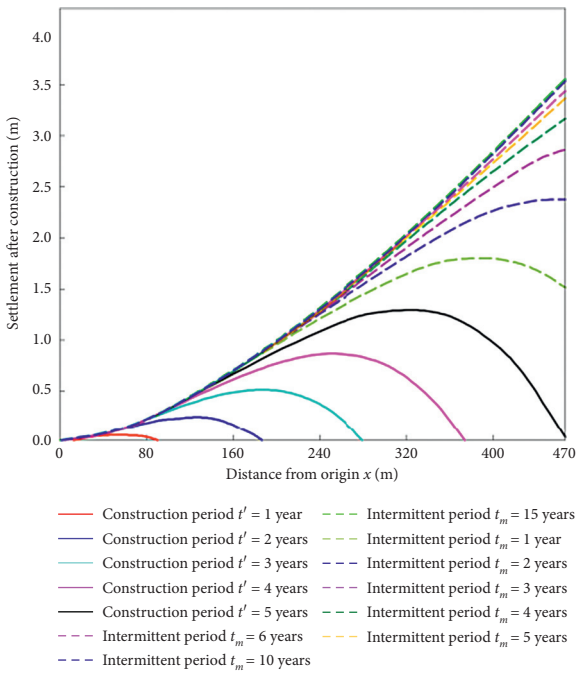

Figure 23: Postwork settlement curve after construction and interval period.

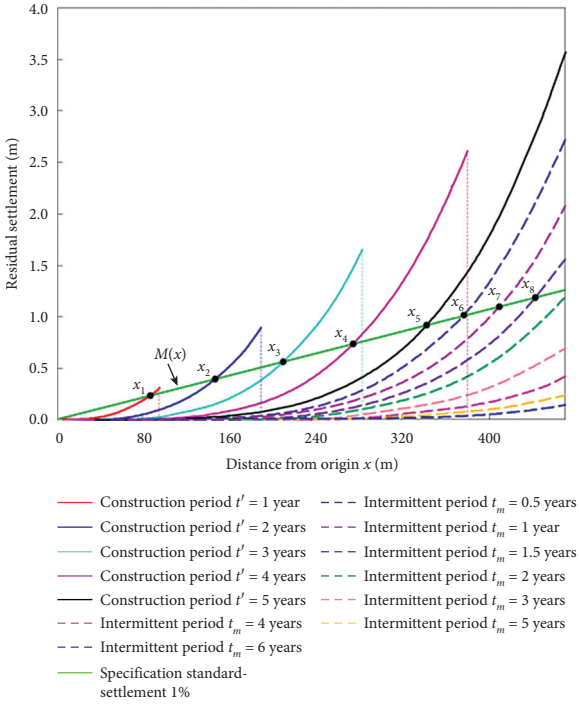

Figure 24: The relation between the settlement control standard of fill code and the propelling position.

of residual settlement intersects with the standard settlement value in different construction periods and intervals. This indicates that, during each construction period and interval, it corresponds to the maximum settlement value of the soil mass measured by the normative safety standard of the fill body, and the intersection point is, respectively, expressed as x_1~x_8. According to this standard, the maximum position of the platform at the top of the filling body occupied by the river can be obtained during the construction period and the interval. The corresponding relationship between the maximum position of the standard settlement and the position of the filling propulsion is shown in Table 2. From the perspective of standard settlement, when the advance position of dumping soil is 376 m, the construction of river course begins, and the residual settlement of the river course and the soil at the bottom of the river bank is within the scope of the standard, which indicates that it is feasible to put all the river courses on the internal dump site.

6. Conclusions

Numerical calculation and field monitoring methods are used to study the deformation law of dump and the optimization method of overlying river parameters in a open-pit coal mine. Some conclusions can be drawn as follows:

(1) The Burgers creep model was applied to the high fill body in a waste dump, and the vertical direction of the dump was stratified. The constitutive equation suitable for the settlement of the dump was put forward. Settlement monitoring analysis of the west dump shows that the height of measuring points 6-1 and 8-1 is 85.5 m and 132.4 m, respectively, and the final settlement after construction is 2.42 m and 3.74 m, respectively. Within 0–1.6 years after soil discharge, the settlement displacement rate of the measuring point increases rapidly; within 1.6–3.7 years, the settlement displacement rate decreases to a certain extent; but after 4 years of soil discharge, the settlement displacement rate basically tends to be stable.

(2) Based on the field monitoring and numerical calculation results, there is a big difference between the numerical results and the field monitoring results in the attenuation creep stage of the creep process in the inversion process of fine-grained soil sand parameters. In the steady-state creep stage, the numerical calculation is consistent with the field monitoring results, and the settlement displacement tends to be stable with time increasing. When the dumping time is 7.96 years, the numerical calculation and field monitoring of the settlement displacement of the measuring point are 3.84 m and 3.68 m, respectively, with a small error between the numerical calculation and monitoring results.

(3) The numerical calculation results of section No. 26 show that the higher the fill height, the longer the stabilization time, and the higher the settlement after construction. Based on the analysis of the influence of the position of filling and pushing on the settlement in area A, it is an effective way to shorten the time of discharging and accelerate the realization of discharging. Under the condition of ensuring the stability of the filled soil slope, when the maximum positions occupied by the river course and river bank construction are measuring points A2, A4, A6, A7, A8, and A10, respectively, it is suggested that the locations of

soil dumping and pushing are measuring points A8, B2, B6, B8, B10, and B10, respectively. Moreover, according to the numerical calculation results of each observation point and the empirical settlement function, the relation formula between the maximum position of the top platform and the time of soil filling is established, and an analysis method for the location selection of the river is proposed.

Data Availability

The data used to support the findings of this study are available from the corresponding author upon request.

Conflicts of Interest

The authors declare that there are no conflicts of interest.

Acknowledgments

This study was supported by the China Postdoctoral Science Foundation (2020M680583), the National Postdoctoral Program for Innovative Talent of China (BX20200191), the Excellent Sino-Foreign Youth Exchange Program of China Association for Science and Technology in 2020 (No. 58), and the Shuimu Tsinghua Scholar Program (2019SM058). This study was also supported by the Discipline Innovation Team of Liaoning Technical University (LNTU20TD-07).

References

[1] P. Marescotti, E. Azzali, D. Servida, C. Carbone, G. Grieco, and G. Lucchetti, "Mineralogical and geochemical spatial analyses of a waste-rock dump at the libiola fe-cu sulphide mine (eastern liguria, Italy)," *Environmental Earth Sciences*, vol. 61, no. 1, pp. 187–199, 2010.

[2] V. I. Cheskidov, V. K. Norri, G. G. Sakantsev, K. Karlstromc, and G. Gehrelsd, "Diversification of open pit coal mining with draglining," *Journal of Mining Science*, vol. 50, no. 4, pp. 690–695, 2014.

[3] V. Ranjan, P. Sen, D. Kumar, and A. Saraswat, "Enhancement of mechanical stability of waste dump slope through establishing vegetation in a surface iron ore mine," *Environmental earth Sciences*, vol. 76, no. 1, pp. 1–9, 2017.

[4] S. Hasani, O. Asghari, F. Doulati Ardejani, and S. Yousefi, "Spatial modelling of hazardous elements at waste dumps using geostatistical approach: a case study Sarcheshmeh copper mine, Iran," *Environmental Earth Sciences*, vol. 76, no. 15, pp. 1–13, 2017.

[5] D. J. Xu, W. Z. Ren, and Q. P. Ren, "Harnessing of landslide for the rock slope in yongping copper mine," *Rock and Soil Mechanics*, vol. 1, pp. 1–10, 1994, in Chinese.

[6] J. Yang, Z. Tao, and B. Li, "Stability assessment and feature analysis of slope in nanfen open pit iron mine," *International Journal of Mining Science and Technology*, vol. 22, no. 3, pp. 329–333, 2012, in Chinese.

[7] S. S. Gupte, R. Singh, V. Vishal, and T. N. Singh, "Detail investigation of stability of in-pit dump slope and its capacity optimization," *International Journal of Earth Sciences and Engineering*, vol. 6, no. 2, pp. 146–159, 2013.

[8] Z. Chen and D. Song, "Numerical investigation of the recent Chenhecun landslide (Gansu, China) using the discrete element method," *Natural Hazards*, vol. 105, no. 1, pp. 717–733, 2020.

[9] Z. Chen, D. Song, M. Juliev, and H. R. Pourghasemi, "Landslide susceptibility mapping using statistical bivariate models and their hybrid with normalized spatial-correlated scale index and weighted calibrated landslide potential model," *Environmental Earth Sciences*, vol. 80, no. 8, p. 324, 2021.

[10] D. Song, X. Liu, Z. Chen, J. Chen, and J. Cai, "Influence of tunnel excavation on the stability of a bedded rock slope: a case study on the mountainous area in southern Anhui, China," *KSCE Journal of Civil Engineering*, vol. 25, no. 1, pp. 114–123, 2021.

[11] D. Song, X. Liu, J. Huang, E. Wang, and J. Zhang, "Characteristics of wave propagation through rock mass slopes with weak structural planes and their impacts on the seismic response characteristics of slopes: a case study in the middle reaches of Jinsha River," *Bulletin of Engineering Geology and the Environment*, vol. 80, no. 2, pp. 1317–1334, 2021.

[12] L. Xiangfeng, Z. Hongyuan, W. Zhenwei, and C. Yue, "Movement and failure law of slope and overlying strata during underground mining," *Journal of Geophysics and Engineering*, vol. 15, no. 4, pp. 1638–1650, 2018.

[13] G. Ma, X. Hu, Y. Yin, G. Luo, and Y. Pan, "Failure mechanisms and development of catastrophic rockslides triggered by precipitation and open-pit mining in emei, sichuan, China," *Landslides*, vol. 15, no. 7, pp. 1401–1414, 2018.

[14] J. Lv, Y. Han, C. Nan, and R. Bai, "The law of deformation and fracture of ground surface and overlying strata with underground mining coal seam compressed at end slope in heidaigou open-pit mine," *Journal of Mining & Safety Engineering*, vol. 36, no. 3, pp. 535–541, 2019, in Chinese.

[15] J. Li, F. Li, M. Hu, X. Zhou, and Y. Huo, "Dynamic monitoring of the mining-induced fractured zone in overburden strata, based on geo-electrical characteristics," *Arabian Journal of Geosciences*, vol. 12, no. 14, 2019.

[16] D. Song, X. Liu, J. Huang, and J. Zhang, "Energy-based analysis of seismic failure mechanism of a rock slope with discontinuities using Hilbert-Huang transform and marginal spectrum in the time-frequency domain," *Landslides*, vol. 18, no. 1, pp. 105–123, 2021.

[17] D. Q. Song, X. L. Liu, J. Huang, Y. F. Zhang, and B. N. Nkwenti, "Seismic cumulative failure effects on a reservoir bank slope with a complex geological structure considering plastic deformation characteristics using shaking table tests," *Engineering Geology*, vol. 286, Article ID 106085, 2021.

[18] D. Song, X. Liu, B. Li, J. Zhang, and J. J. V. Bastos, "Assessing the influence of a rapid water drawdown on the seismic response characteristics of a reservoir rock slope using time-frequency analysis," *Acta Geotechnica*, vol. 16, no. 4, pp. 1281–1302, 2021.

[19] M. Marschalko, I. Yilmaz, K. Kubečka et al., "Utilization of ground subsidence caused by underground mining to produce a map of possible land-use areas for urban planning purposes," *Arabian Journal of Geosciences*, vol. 8, no. 1, pp. 579–588, 2015.

[20] C. Piao, D. Wang, H. Kang, H. He, C. Zhao, and W. Liu, "Model test study on overburden settlement law in coal seam backfill mining based on fiber Bragg grating technology," *Arabian Journal of Geosciences*, vol. 12, no. 13, pp. 1–9, 2019.

[21] Z. Chang, J. Wang, M. Chen, Z. Ao, and Q. Yao, "A novel ground surface subsidence prediction model for sub-critical

mining in the geological condition of a thick alluvium layer," *Frontiers of Earth Science*, vol. 9, no. 2, pp. 330–341, 2015.

[22] T. Carlà, P. Farina, E. Intrieri, K. Botsialas, and N. Casagli, "On the monitoring and early-warning of brittle slope failures in hard rock masses: examples from an open-pit mine," *Engineering Geology*, vol. 228, pp. 71–81, 2017.

[23] X. Zhu, G. Guo, H. Liu, T. Chen, and X. Yang, ""Experimental research on strata movement characteristics of backfill–strip mining using similar material modeling," *Bulletin of Engineering Geology and the Environment*, vol. 78, no. 4, pp. 2151–2167, 2019.

[24] G. J. Dick, E. Graham, E. Eberhardt, A. G. Cabrejo-Liévano Stead, D. Stead, and N. D. Rose, Development of an early-warning time-of-failure analysis methodology for open-pit mine slopes utilizing ground-based slope stability radar monitoring data," *Canadian Geotechnical Journal*, vol. 52, no. 4, pp. 515–529, 2015.

[25] F. Zhang, T. Yang, L. Li et al., "Cooperative monitoring and numerical investigation on the stability of the south slope of the Fushun west open-pit mine," *Bulletin of Engineering Geology and the Environment*, vol. 78, no. 4, pp. 2409–2429, 2019.

[26] G.-w. Liu, D.-q. Song, Z. Chen, and J.-w. Yang, "Dynamic response characteristics and failure mechanism of coal slopes with weak intercalated layers under blasting loads," *Advances in Civil Engineering*, vol. 2020, pp. 1–18, Article ID 5412795, 2020.

[27] H. Du, D. Song, Z. Chen, and Z. Guo, "Experimental study of the influence of structural planes on the mechanical properties of sandstone specimens under cyclic dynamic disturbance," *Energy Science & Engineering*, vol. 8, no. 11, pp. 4043–4063, 2020.

[28] D. Song, Z. Chen, H. Chao, Y. Ke, and W. Nie, "Numerical study on seismic response of a rock slope with discontinuities based on the time-frequency joint analysis method," *Soil Dynamics and Earthquake Engineering*, vol. 133, Article ID 106112, 2020.

[29] D. Song, Z. Chen, Y. Ke, and W. Nie, "Seismic response analysis of a bedding rock slope based on the time-frequency joint analysis method: a case study from the middle reach of the Jinsha River, China," *Engineering Geology*, vol. 274, Article ID 105731, 2020.

[30] X. L. Liu and S. Y. Wang, "Mine water inrush forecasting during the mining under waters," *Disaster Advances*, vol. 5, no. 4, pp. 877–882, 2012.

[31] X. Liu, S. Wang, S. Wang, and E. Wang, "Fluid-driven fractures in granular materials," *Bulletin of Engineering Geology and the Environment*, vol. 74, no. 2, pp. 621–636, 2015.

[32] Q. Du, X. Liu, E. Wang, and S. Wang, "Strength reduction of coal pillar after CO2 sequestration in abandoned coal mines," *Minerals*, vol. 7, no. 2, p. 26, 2017.

[33] P. Lin, X. Liu, S. Hu, and P. Li, "Large deformation analysis of a high steep slope relating to the laxiwa reservoir, China," *Rock Mechanics and Rock Engineering*, vol. 49, no. 6, pp. 2253–2276, 2016.

[34] C. Liu, X. Liu, X. Peng, E. Wang, and S. Wang, "Application of 3D-DDA integrated with unmanned aerial vehicle-laser scanner (UAV-LS) photogrammetry for stability analysis of a blocky rock mass slope," *Landslides*, vol. 16, no. 9, pp. 1645–1661, 2019.

[35] K. Gao, S.-N. Li, R. Han et al., "Study on the propagation law of gas explosion in the space based on the goaf characteristic of coal mine," *Safety Science*, vol. 127, Article ID 104693, 2020.

[36] C. Xia, L. Jin, and R. Guo, "Nonlinear theoretical rheological model for rock: a review and some problems," *Yanshilixue Yu Gongcheng Xuebao/Chinese" Journal of Rock Mechanics and Engineering*, vol. 30, no. 3, pp. 454–463, 2011.

[37] W. W. Du, "Settlement displacement calculation of horizontal foundation dump," *Mining and Metallurgical Engineering*, vol. 1, pp. 2–5, 1990, in Chinese.

[38] K. Wu, Z. Shao, and S. Qin, "An analytical design method for ductile support structures in squeezing tunnels," *Archives of Civil and Mechanical Engineering*, vol. 20, no. 3, p. 91, 2020.

[39] K. Wu, Z. Shao, S. Qin, N. Zhao, and H. Hu, "Analytical-based assessment of effect of highly deformable elements on tunnel lining within viscoelastic rocks," *International Journal of Applied Mechanics*, vol. 12, no. 3, Article ID 2050030, 2020.

[40] K. Wu, Z. Shao, S. Qin, W. Wei, and Z. Chu, "A critical review on the performance of yielding supports in squeezing tunnels," *Tunnelling and Underground Space Technology*, vol. 114, Article ID 103815, 2021.

[41] H. Du, D. Song, Z. Chen, H. Shu, and Z. Guo, "Prediction model oriented for landslide displacement with step-like curve by applying ensemble empirical mode decomposition and the PSO-ELM method," *Journal of Cleaner Production*, vol. 270, Article ID 122248, 2020.

[42] H. Du, D. Song, Z. Chen, and Z. Z. Guo, "Experimental study of the influence of structural planes on the mechanical properties of sandstone specimens under cyclic dynamic disturbance," *Engineering Science & Engineering*, vol. 8, no. 11, pp. 4043–4063, 2020.

[43] Z. Deng, N. Liang, X. Liu, A. de la Fuente, P. Lin, and H. Peng, "Analysis and application of friction calculation model for long-distance rock pipe jacking engineering," *Tunnelling and Underground Space Technology*, vol. 115, Article ID 104063, 2021.

[44] Z. Deng, X. Liu, P. Chen et al., "Basalt-polypropylene fiber reinforced concrete for durable and sustainable pipe production. Part 1: Experimental Program," *Structural Concrete*, 2021.

[45] Z. Deng, X. Liu, X. Yang et al., "A study of tensile and compressive properties of hybrid basalt-polypropylene fiber-reinforced concrete under uniaxial loads," *Structural Concrete*, 2020.